Pergamon

Acta mater. 48 (2000) 4181–4189

Acta MATERIALIA

www.elsevier.com/locate/actamat

WORK HARDENING IN HETEROGENEOUS ALLOYS—A MICROSTRUCTURAL APPROACH BASED ON THREE INTERNAL STATE VARIABLES

F. ROTERS[1], D. RAABE[1] and G. GOTTSTEIN[2]*

[1]Max-Planck-Institut für Eisenforschung, D-40237 Düsseldorf, Germany and [2]Institut für Metallkunde und Metallphysik, Collaborative Research Centre 370 "Integral Modelling of Materials" of the DFG, RWTH Aachen, D-52056 Aachen, Germany

(Received 7 April 2000; received in revised form 9 August 2000; accepted 9 August 2000)

Abstract—A new work-hardening model for homogeneous and heterogeneous cell-forming alloys is introduced. It distinguishes three internal state variables in terms of three categories of dislocations: mobile dislocations, immobile dislocations in the cell interiors and immobile dislocations in the cell walls. For each dislocation population an evolution law is derived taking into account dislocation generation, annihilation and storage by dipole and lock formation. In particular, these rate equations take into account the number of active glide systems and, thus, introduce texture in the model in addition to the Taylor factor. Microstructure is represented by the dislocation cell structure as well as second-phase particles, which may undergo changes by precipitation and Ostwald ripening. Interaction of mobile dislocations with the microstructure is taken into account through an effective slip length of the mobile dislocations.

For the same set of parameters, the predictions are in excellent agreement with measured stress–strain curves of both a precipitation-hardened aluminium alloy (Al–4.16 wt% Cu–1.37 wt% Mg, AlCuMg2) and a precipitation-free model alloy (Al–0.35 wt% Cu–0.25 wt% Mg), the composition of which corresponds to the matrix of the two-phase alloy. © *2000 Acta Metallurgica Inc. Published by Elsevier Science Ltd.*

Zusammenfassung—Ein neues Verfestigungsmodell für homogene und heterogene Legierungen wird vorgestellt. Es werden drei innere Zustandsvariablen in Form von drei Versetzungsklassen unterschieden, mobile Versetzungen, immobile Versetzungen im Zellinnern und immobile Versetzungen in den Zellwänden der Substruktur. Für die Dichte jeder dieser Versetzungsklassen wird eine Evolutionsgleichung hergeleitet, die Versetzungsproduktion, -annihilation und -speicherung durch Bildung von Dipolen und seßhaften Versetzungsreaktionsprodukten berücksichtigt. Insbesondere wird dabei die Zahl der aktiven Gleitsysteme berücksichtigt, wodurch die Textur zusätzlich zum Taylorfaktor in das Modell einfließt. Die Mikrostruktur wird durch die Versetzungszellstruktur und Sekundärphasen repräsentiert, wobei letztere Ausscheidungs- und Reifungsprozessen unterworfen sind. Die Wechselwirkung der mobilen Versetzungen mit der Mikrostruktur wird durch eine effektive freie Weglänge der mobilen Versetzungen berücksichtigt.

Die Modellvorhersagen stimmen bei gleichem Parametersatz sehr gut mit gemessenen Spannungs-Dehnungs-Kurven einer ausscheidungshärtbaren Aluminiumlegierung (Al–4.16 wt% Cu–1.37 wt% Mg, AlCuMg2) und einer ausscheidungsfreien Modellegierung (Al–0.35 wt% Cu–0.25 wt% Mg), die der Matrix des zweiphasigen Werkstoffs entspricht, überein. © *2000 Acta Metallurgica Inc. Published by Elsevier Science Ltd.*

Keywords: Alloys, aluminium; Dislocations, theory; Mechanical properties, plastic; Dislocations, mobility

1. INTRODUCTION

For a more precise modelling of forming processes, e.g., by finite element (FE) codes, accurate prediction of the strain-hardening behaviour is required. In the majority of FE codes the hardening behaviour of commercial alloys is represented by empirical relationships, mostly in terms of power laws of strain and strain rate. Despite their remarkably good fit to measured stress–strain curves, empirical relations have no predictive power beyond the measured range of deformation conditions and material chemistry. In particular, such models use macroscopic quantities as state parameters like strain or chemical composition to describe the mechanical behaviour of a material. This is fundamentally wrong, however, since the mechanical properties depend on microstructure rather than on overall chemistry, and thus are liable

* To whom correspondence should be addressed. Tel.: 00 49 241 806 860; fax: 00 49 241 8888 608.
E-mail address: gg@imm.rwth—aachen.de (G. Gottstein)

1359-6454/00
PII: S1359-6454(00)00289-5

to change during processing of the material. In fact, an appropriate representation of the hardening behaviour has to be based on microstructural state variables which are affected by the processing history of the material. There are micromechanical models that contain explicit internal state variables, like the models of Robinson and Bartolotta [1] or Chaboche [2], which have been successfully implemented in finite element codes. Although such approaches do define evolutionary equations for the internal state variables, the respective constants are commonly used as fit parameters and do not relate to specific mechanisms of microstructure evolution.

There have been numerous attempts in the past to predict work-hardening behaviour in terms of dislocation concepts, with limited success, however, with regard to correctly predicting hardening behaviour in a wide field of temperature, strain rate and material chemistry. In the current study, we present a model based on contemporary understanding of microstructural evolution and the interaction of dislocations with microstructural essentials. It will be shown that such a model gives a reasonable description of the hardening behaviour and accounts adequately for changes of material chemistry, in particular for age-hardened alloys.

For properly testing both parts of the model (i.e., the dislocation–dislocation interaction and the dislocation–precipitate interaction) it is essential to separate the two effects also experimentally. This can be accomplished by using a single-phase alloy that represents the matrix material of the corresponding precipitation-hardened alloy.

The structure of the paper is as follows. First, we present the three-variable concept and its evolution laws. Second, the physical parameters are adjusted in the allowed range to fit the measured stress–strain curve of the single-phase model alloy. Third, the same set of parameters is used to model the stress–strain curve of the precipitation-hardened alloy by optimizing just the parameters for the description of precipitation that were not used for simulating the model alloy as it is free of precipitates.

2. THE THREE-INTERNAL-VARIABLES MODEL

2.1. The concept

We confine our consideration to cell/subgrain-forming metals and alloys, which includes most commercial aluminium alloys, copper and nickel alloys as well as steels. With progressing strain a cellular dislocation arrangement develops, composed of cell walls with high dislocation density (ρ_w) which enclose cell interiors of low dislocation density (ρ_i). Dislocation sources inside the material generate mobile dislocations (ρ_m), which interact with dislocations in the cell interior and dislocations in the cell walls upon their way through the crystal forced by the applied stress to accommodate the imposed strain. This interaction can result in the formation of dislocation dipoles or even annihilation of dislocations. Dipoles will finally be swept into the dislocation walls, where they are subject to thermally activated recovery processes.

Interior dislocation sources will emit dislocation loops. If we consider the loops to be of square shape with length $2L$, we represent the loop expansion by the motion of one of its segments, more specifically an edge dislocation segment. Hence, we have to keep in mind that a slip length L corresponds to a total dislocation loop length of $8L$ and a swept area of $(2L)^2$. While in the real world a loop will percolate through its slip plane and leave debris behind around circumvented impenetrable areas, we follow the classical analogon and assume instead that the considered dislocation segment will cease to move after a slip length L. This slip length is determined by obstacles which the mobile dislocations encounter on their way through the crystal. Such obstacles will be other dislocations, grain boundaries or precipitates, each of which has a specific spacing L_i^{obst}. There is no unique concept to treat the superposition of more than one obstacle type (hardening mechanism) but with increasing obstacle density (smaller obstacle spacing) the slip length must decrease. This can be accounted for by the assumption

$$\frac{1}{L} = \sum_i \frac{w_i}{L_i^{\text{obst}}} \tag{1}$$

(where w_i is a weight factor), since this will adjust the slip length to be dominated by the shortest spacing among the competing obstacles.

Of course, this does not account for different obstacle strength or the local dislocation arrangement due to the dislocation–obstacle interaction (e.g., geometrically necessary dislocations next to non-deformable particles), but it reflects an effective influence of the ensemble of obstacles.

With regard to recovery processes, we limit our consideration to the climb of edge dislocations, since we primilary consider elevated-temperature behaviour (hot-forming). Cross-slip of screw segments will be accounted for in an extended version of the model when, in particular, low-temperature behaviour is of concern.

All dislocation-hardening models are single-crystal models in their fundamental set-up. The extension to polycrystal behaviour is accomplished by introduction of the Taylor factor M, which relates the macroscopically imposed strain $d\epsilon$ to the total slip on all active glide systems in the grains $\Sigma d\gamma$, and thus the macroscopic flow stress σ to the acting shear stress τ in the slip systems,

$$\sigma = M\tau = \frac{\sum \mathrm{d}\gamma}{\mathrm{d}\epsilon}\tau. \tag{2}$$

In polycrystals, besides the Taylor factor, the grain size is introduced in the effective slip length equation [equation (1)] to account for the limited crystallite dimensions.

2.2. The model

2.2.1. Kinetic equation of state. The basic structure of the three-internal-variables model (3IVM) consists of a kinetic equation of state and a set of equations for the structure evolution as do many other dislocation models of crystal plasticity [3–13]. In extension of the various statistical one- [3–6] and two- [7–13] variable models, the 3IVM suggested here distinguishes three dislocation categories (see Fig. 1): namely, mobile dislocations (ρ_m), immobile dislocations in the cell interiors (ρ_i) and immobile dislocations in the cell walls (ρ_w). For each class of dislocations an evolutionary law of the form

$$\dot{\rho}_x = \dot{\rho}_x^{+} - \dot{\rho}_x^{-} \tag{3}$$

will be derived below, where the index x assumes either m (mobile), i (cell interior) or w (cell wall). The $\dot{\rho}_x^{+}$ term represents one or more production terms while $\dot{\rho}_x^{-}$ represents the reduction terms.

The kinetic equation of state is used to calculate the required external stress σ_ext to comply with the imposed strain rate $\dot{\epsilon}$ for a given structure and temperature. Within the 3IVM, the Orowan equation

$$\dot{\gamma} = \dot{\epsilon}M = \rho_\mathrm{m} b v \tag{4}$$

will be used as kinetic equation of state. In equation (4), $\dot{\gamma}$ is the shear rate, M the Taylor factor of the polycrystalline material for the imposed strain path, and b the magnitude of the Burgers vector. Use of the Taylor factor to relate the macroscopic strain rate to the dislocation behaviour in the crystals implies, of course, that the dislocation properties are considered as population average values. The average dislocation glide velocity v depends on the effective stress $\tau_\mathrm{eff} = \tau - \hat{\tau}$, where τ is the acting shear stress and $\hat{\tau}$ is the athermal flow stress.

$$v = \lambda \nu_0 \exp\left(-\frac{Q}{\mathrm{k}_B T}\right) \sinh\left(\frac{\tau_\mathrm{eff} V}{\mathrm{k}_B T}\right), \tag{5}$$

where λ is the jump width—i.e., the mean spacing of obstacles (the immobile forest dislocations in this case), ν_0 is the attack frequency*, Q is the effective activation energy for dislocation glide, and V is the activation volume. In commercial alloys the solute atoms present in the matrix result in higher values for Q than those used for pure metals. Substituting equation (5) into equation (4), equation (4) can be solved for τ_eff.

As the forest dislocation spacing is different in the cell interior and the cell walls, one obtains two different values for the effective stress, τ_{eff_i} in the cell interiors and τ_{eff_w} in the cell walls. In both cases the passing stress of dislocations has to be added to derive the necessary resolved shear stress in the cell interior τ_i and in the cell walls τ_w

$$\tau_x = \tau_{\mathrm{eff}_x} + \alpha G b \sqrt{\rho_x}, \quad x = \mathrm{i}, \mathrm{w} \tag{6}$$

with α being a constant and G being the shear modulus, both of which are mildly temperature-dependent. The required external stress can then be calculated as [5, 6]

$$\sigma_\mathrm{ext} = M(f_\mathrm{i}\tau_\mathrm{i} + f_\mathrm{w}\tau_\mathrm{w}), \tag{7}$$

where M is again the Taylor factor for polycrystalline material, which can be calculated for arbitrary strain paths as a function of the total strain [15], and f_i, f_w

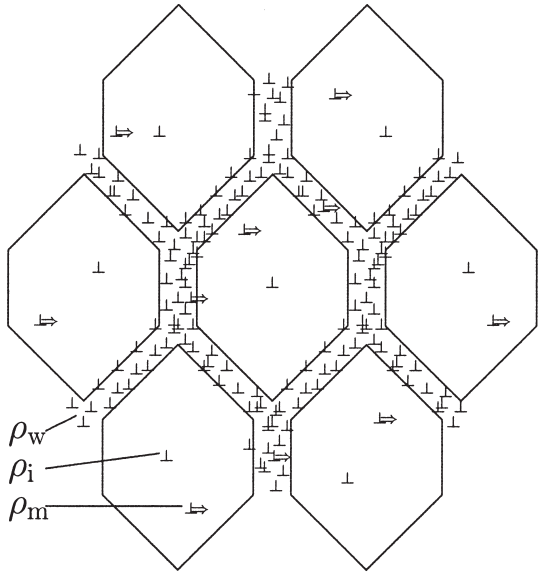

Fig. 1. Schematic drawing of the arrangement of the three dislocation classes considered in the three-internal-variables model: mobile dislocations (ρ_m), immobile dislocations in the cell interiors (ρ_i) and immobile dislocations in the cell walls (ρ_w).

* There are different approaches for the attack frequency, either inversely proportional to the obstacle spacing or independent of obstacle spacing. Throughout the paper we assume the attack frequency to be constant in line with internal friction results [14].

are the volume fractions of cell interior and cell walls, respectively.

2.2.2. Structure evolution equations. While the kinetic equation of state determines the flow stress for a given structure, a set of structure evolution laws is needed to calculate stress–strain curves. In this section an evolution law will be derived for each of the dislocation densities considered in the model based on the underlying elementary dislocation processes.

The mobile dislocations carry the plastic strain. They are assumed to penetrate both dislocation walls and cell interiors. Each mobile dislocation is supposed to travel a mean free path L_{eff} before it is immobilized or annihilated by one of the processes outlined below. A relationship between the imposed strain and the mobile dislocation density is obtained if the Orowan equation is considered on a larger time scale. In a time increment Δt, a dislocation density $\dot{\rho}_{\text{m}}^{+}\,\Delta t$ is produced and immobilized after travelling the distance L_{eff}. This is associated with a strain increment $\Delta\epsilon$, so

$$\frac{\Delta\epsilon}{\Delta t} \cong \dot{\epsilon} = \dot{\rho}_{\text{m}}^{+}\, b L_{\text{eff}} \frac{1}{M}. \tag{8}$$

L_{eff} is determined by the effective grain size* K and three obstacle spacings: the forest dislocation spacing in the cell walls L_{w}, the forest dislocation spacing in the cell interior L_{i}, and the spacing of the precipitates L_{p}. The calculation of L_{p} and why it is introduced at this point will be discussed separately below.

As outlined in Section 2.1, it is difficult to define an effective obstacle spacing if more than a single obstacle type interacts with the moving dislocations with different strength. From the reasons given in Section 2.1, we arrive at

$$\frac{1}{L_{\text{eff}}} = \frac{\beta_{\text{i}}}{L_{\text{i}}} + \frac{\beta_{\text{w}}}{L_{\text{w}}} + \frac{1}{K} + \frac{1}{L_{\text{p}}(t)}, \tag{9}$$

where β_{i} and β_{w} are constants, which relate the spacing of the respective dislocations (i, w) to the slip length, if only this type of dislocation would determine the slip distance L_{eff}. We assume the mobile dislocation density to be reduced by three processes; namely, by the formation of dislocation dipoles† and dislocation locks as well as by annihilation. For each process a probability for the decrease of dislocation density can be derived, as will be shown below in detail for the annihilation process.

Assuming that spontaneous *annihilation* takes place when two dislocations with antiparallel Burgers vectors come closer to each other than a critical distance $d_{\text{annihil-c}}$, the probability for the event can be calculated according to Fig. 2. During a time increment dt a mobile dislocation travels a distance v dt. Thus, spontaneous annihilation will take place if there is a suitable dislocation within the area $2d_{\text{annihil-c}}v\,\text{d}t$ (shaded area in Fig. 2). The number dp of mobile dislocations to serve as reaction partner within this area reads

$$\text{d}p = 2d_{\text{annihil - c}} v\,\text{d}t\rho_{\text{m}}. \tag{10}$$

However, for an annihilation event to take place, it is required to find an antiparallel dislocation; i.e., a dislocation on the same glide system. If the number of active glide systems is denoted n, and one assumes an equal density of dislocations on all active glide systems, this gives rise to a normalization term $1/n$ for the probability calculation. Taking into account the number of active glide systems renders the rate equations texture-sensitive. Under the assumption of an equal density of positive and negative dislocations, an additional term 1/2 must be considered as the two reacting dislocations have to be of opposite sign. The reaction rate $\dot{p}$ of an individual moving dislocation now reads

$$\dot{p} = 2d_{\text{annihil - c}} v\rho_{\text{m}} \frac{1}{2n}. \tag{11}$$

The Orowan equation (4) can be used to substitute $v\rho_{\text{m}}$ to yield

$$\dot{p} = 2d_{\text{annihil - c}} \frac{\dot{\epsilon} M}{b}\frac{1}{2n}. \tag{12}$$

For calculating the reduction rate $\dot{\rho}_{\text{m}}^{-}$ of the mobile dislocation density due to annihilation, one has to take into account that, with each annihilation event, two

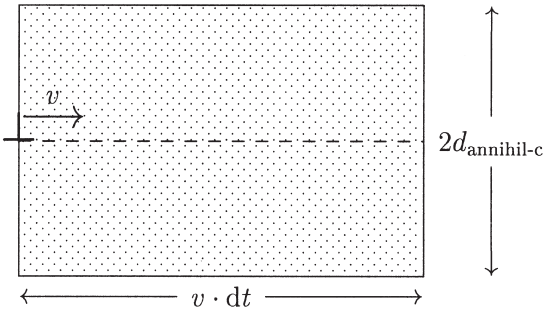

Fig. 2. Geometrical set-up for calculating the annihilation probability.

* The effective grain size is understood to be some constant fraction of the true grain size.

† Note that dislocation dipoles can still be moved [16]. But since the motion of dislocation dipoles does not contribute to the net strain, they are no longer considered in the class of mobile dislocations.

dislocations are eliminated and that the density of mobile dislocations is ρ_m

$$\dot{\rho}_m^-(\text{annihil}) = 2\dot{p}\rho_m = 2d_{\text{annihil - c}}\frac{\dot{\epsilon}M1}{b\ n}\rho_m. \quad (13)$$

The formation of dislocation *locks* can be derived analogously. For this, the critical distance for the spontaneous formation of locks becomes d_{lock} instead of $d_{\text{annihil-c}}$. Moreover, since reaction partners can be dislocations on all other active glide systems, this leads to a factor $(n-1)/n$ instead of $1/n$. The reduction rate of the dislocation density $\dot{\rho}_m^-$ due to the formation of locks then reads

$$\dot{\rho}_m^-(\text{lock}) = 4d_{\text{lock}}\frac{\dot{\epsilon}M}{b}\frac{n-1}{n}\rho_m. \quad (14)$$

The third process taken into account is the formation of *dipoles*. Again, the derivation is very similar to that for annihilation. For a dipole to form the distance between the two dislocations has to exceed the critical distance for annihilation $d_{\text{annihil-c}}$ but has to be small enough to have the involved dislocations trap each other. For this to happen, the acting resolved shear stress due to the external stress has to be balanced by the stress field of the individual dislocations. This implies that the critical spacing for the formation of dipoles (d_{dipol}) scales inversely with the externally applied stress. The respective area that has to be considered amounts to $2(d_{\text{dipol}}-d_{\text{annihil - c}})v\,\text{d}t$ (shaded area in Fig. 3). The reduction rate $\dot{\rho}_m^-$ due to the formation of dipoles then reads

$$\dot{\rho}_m^-(\text{dipol}) = 2(d_{\text{dipol}}-d_{\text{annihil - c}})\frac{\dot{\epsilon}M1}{b\ n}\rho_m. \quad (15)$$

The second category of dislocations considered are the *immobile dislocations* in the cell interiors ρ_i. The rate of increase of the dislocation density inside the cells $\dot{\rho}_i^+$ is equal to the decrease of mobile dislocations due to the formation of locks, which was derived in the previous section [equation (14)]

$$\dot{\rho}_i^+ = \dot{\rho}_m^-(\text{lock}) = 4d_{\text{lock}}\frac{\dot{\epsilon}M}{b}\frac{n-1}{n}\rho_m. \quad (16)$$

Since locks cannot glide, the only process to decrease the immobile dislocation density is annihilation by dislocation climb. The velocity of climb v_{climb} is diffusion-controlled

$$v_{\text{climb}} = \frac{D}{k_B T}\tau A, \quad (17)$$

where D is the self-diffusion coefficient, and A the activation area. The rate equation for this process is then given by

$$\dot{\rho}_i^- = 2v_{\text{climb}}d_{\text{annihil - g}}\frac{1}{n}\rho_i^2. \quad (18)$$

The third class of dislocations are the immobile dislocations in the cell walls ρ_w. These dislocations undergo the same processes as those in the cell interiors, but there is one additional process, which contributes to the increase of this particular dislocation density. According to Kratochvíl and Libovický [16], it can be assumed that all dislocation dipoles finally end up and accumulate in the cell walls. As dipoles are created in the whole volume, but stored in the walls only, the rate of increase amounts to

$$\dot{\rho}_w^+ = \frac{1}{f_w}\dot{\rho}_m^-(\text{dipol}) = \frac{1}{f_w}2(d_{\text{dipol}} - d_{\text{annihil - c}})\frac{\dot{\epsilon}M1}{b\ n}\rho_m. \quad (19)$$

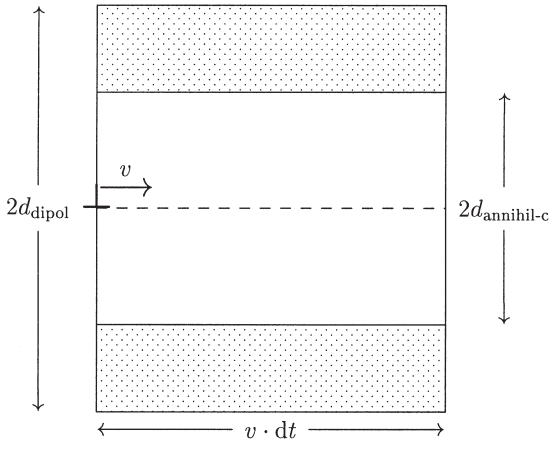

Fig. 3. Geometrical set-up for calculating the probability for the formation of dipoles.

2.2.3. Precipitates. Commercial alloys are commonly heterogeneous—i.e., comprise second phases in a solid-solution matrix. Dislocation motion in such systems has to take into account solid solution hardening and precipitation hardening. Shearable precipitates essentially affect the yield stress only, while the hardening behaviour of the respective alloy is akin to that of the pure matrix materials or its solid solution. Non-shearable particles affect plastic flow mainly in two ways. First, they increase the yield stress by the Orowan stress

$$\tau_{\text{OROWAN}} = \frac{Gb\sqrt{V_p}}{r}, \quad (20)$$

where V_p is the volume fraction of precipitates and r

the average precipitate radius. Second, they drastically increase the hardening rate due to the plastic zone (geometrically necessary dislocations) in the wake of the particles. The dislocation concept introduced here does not lend itself easily to accommodate these physical processes, but they can be accounted for qualitatively by the basic equations derived so far. A higher yield stress can be represented by a larger glide resistance as expressed by a larger activation energy Q for glide [equation (5)]. The increased hardening rate is taken care of by modification of the slip length, i.e., by incorporating the precipitate spacing

$$L_p = \frac{r}{\sqrt{V_p}} \tag{21}$$

in the effective slip length as already accounted for in equation (9). In particular, for elevated-temperature deformation, L_p may depend on time, since precipitation and Ostwald ripening may occur during deformation. We follow a concept proposed by Estrin and co-workers [17] to account for this complication. For precipitate coarsening the change of precipitate radius with time is given by

$$r = c(t + t_0)^{1/k}, \tag{22}$$

with c the kinetic constant, t the time, t_0 the time prior to the test, and $k = 3$ for ideal Ostwald ripening according to the Lifshitz–Slyozov–Wagner theory (LSW theory) [18, 19].

If concurrent precipitation occurs the precipitate volume fraction will change, which can be described by an Avrami-type equation [20]

$$V_p = \left\{1 - \exp\left[-\left(\frac{t + t_0}{\hat{t}}\right)^m\right]\right\} V_\infty \tag{23}$$

with an Avrami exponent m and the volume fraction V_∞ of precipitates in thermodynamic equilibrium. The characteristic time is

$$\hat{t} = \frac{A_0}{D} = \frac{A_0}{D_0} \exp\left(\frac{H_m}{k_B T}\right) \tag{24}$$

with A_0 a constant, D the respective diffusion coefficient comprising the pre-exponential term D_0 and the activation enthalpy H_m. The diffusion coefficients are taken for the main alloy components [20].

It is noted that this concept unlawfully mixes two kinetics, namely precipitation and ripening kinetics. Since both processes operate on a different time scale, however, the error introduced is small and mitigated by using effective kinetic constants, e.g., an effective k in equation (22).

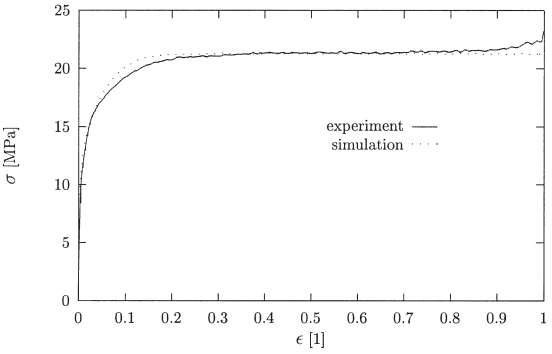

Fig. 4. Modelled and measured stress–strain curves for $\dot{\epsilon} = 1\times10^{-3}\ s^{-1}$ and $T = 350°C$. Single-phase model alloy (Al–0.35 wt% Cu–0.25 wt% Mg).

3. APPLICATIONS

3.1. Experimental

In order to validate the model, hot compression tests were performed at $T = 350°C$ with a strain rate of $\dot{\epsilon} = 10^{-3}\ s^{-1}$ on AlCuMg2 (Al–4.16 wt% Cu–1.37 wt% Mg). The experimental stress–strain curve of the precipitation-hardened aluminium alloy exhibits a characteristic stress peak (solid line in Fig. 5). This maximum is caused by the ripening of precipitates. In order to check this assumption a model alloy (Al–0.35 wt% Cu–0.25 wt% Mg) with reduced copper and magnesium content was also tested. At $T = 350°C$ the model alloy is a homogeneous solid solution with the same composition as the matrix of the two-phase alloy and, thus, can be used to study the properties of the matrix material of the two-phase alloy. It can be seen from Fig. 4 that the stress–strain curve of the model alloy shows a behaviour typical of hardening superimposed by dynamic recovery.

3.2. Single-phase model alloy

In a first step the 3IVM was adapted to the single-phase model alloy. Since the kinetic equation as well as the structure evolution equations contain a variety

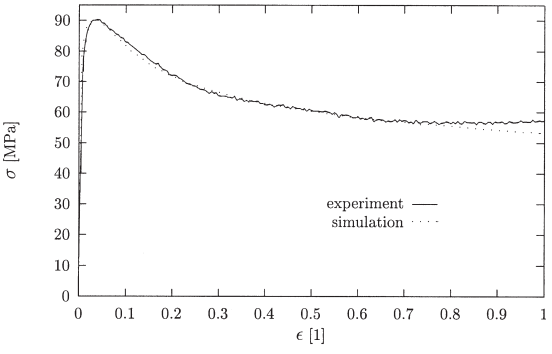

Fig. 5. Modelled and measured stress–strain curves for $\dot{\epsilon} = 1\times10^{-3}\ s^{-1}$ and $T = 350°C$. Precipitation-hardened aluminium alloy (Al–4.16 wt% Cu–1.37 wt% Mg, AlCuMg2).

of physical constants that are not known exactly but in their order of magnitude, they were set to reasonable values before the fitting process. All material constants were chosen for pure aluminium. The volume fractions were set to $f_i = 0.9$ and $f_w = 0.1$. In accordance with the studies of Essman and Mughrabi [21] and Tippelt *et al.* [22], the critical distance for annihilation in the direction of climb was set to $d_{\text{annihil - c}} = 1$ nm. As dislocations have a higher mobility for glide than for climb, both $d_{\text{annihil-g}}$ and d_{lock} were set to 5 nm. The attack frequency was chosen as $f = 7.8\times10^9$ Hz [14]. The initial value of all three dislocation densities was 10^{10} m^{-2}. As compression tests were modelled, an average Taylor factor of $M = 3.06$ was used for all simulations. Texture change during deformation was not taken into account.

The remaining parameters were optimized to obtain the lowest possible value for the mean square deviation of measured and simulated stress–strain curves. For the fitting process the experimental data were used only up to a strain of $\epsilon = 0.7$, because at larger strains the influence of friction became dominant, which was not accounted for in the simulation. It can be seen from Fig. 4 that the simulated stress–strain curve (dashed line in Fig. 4), which is predicted by using the 3IVM without consideration of precipitation, is in very good accord with the experimental curve (solid line). The mean deviation amounts to less than 3%.

The optimization process yielded the following values: effective grain size $K = 10$ μm, which is 10% less than the average grain size; number of active glide systems $n = 3$, this value may seem too low as five active glide systems are necessary for compatible deformation, however Kocks and Canova [23] showed that this is true only in the direct vicinity of the grain boundaries and that the number of active glide systems is lower in most of the crystal volume; activation energy for dislocation glide $Q = 1.96$ eV, looking at equation (5) this value could be expected to be much lower as the activation energy for forest cutting is of the order $Gb^3/4\pi$. But it has to be taken into account that the model alloy is not a pure metal and the solute atoms result in an increase of the yield stress which can be represented by higher values for Q (see Section 2.2.3). Secondly, many of the mobile dislocations are jogged rather than ideal straight dislocations. Therefore, the activation energy for the movement of jogs has to be taken into account as well, and Q actually is an effective activation energy for dislocation glide which is impossible to predict without making additional assumptions on the exact dislocation configuration.

3.3. AlCuMg2

In a second step the stress–strain curve for the precipitation-hardened alloy was modelled using the same set of parameters with additional consideration of precipitation kinetics.

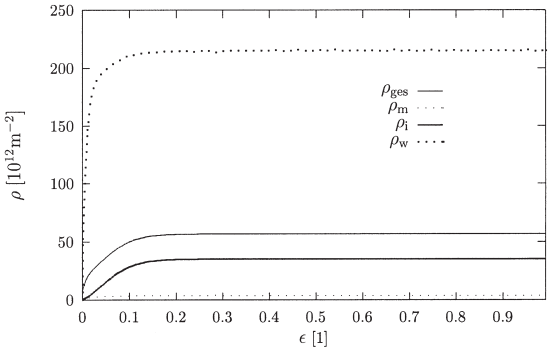

Fig. 6. Modelled dislocation densities for $\dot{\epsilon} = 1\times10^{-3}$ s^{-1} and $T = 350°$ C. Single-phase model alloy (Al–0.35 wt% Cu–0.25 wt% Mg).

The diffusional data for precipitation were taken as that of copper in aluminium. The equilibrium volume fraction of precipitates V_∞ amounts to about 0.06. Optimizing the other parameters of equations (22)–(24) for the precipitation and coarsening kinetics ($A_0 = 1.1\times10^{-14}$, $m = 1.4$, $c = 6.0\times10^{-9}$, $k = 2.3$, $t_0 = 0$ s) leads to a curve with a well-defined stress maximum (Fig. 5). A comparison of the resulting curve with the experimental data for AlCuMg2 shows again very good agreement with a mean deviation of about 7%.

3.4. Dislocation densities

Figures 6 and 7 illustrate the evolution of the dislocation densities with strain. The shape of the curves for the total dislocation densities, $\rho_{\text{ges}} = f_i\rho_i + f_w\rho_w + \rho_m$, is in both cases quite similar to the shape of the stress–strain curve. In the case of the single-phase alloy all dislocation densities reach their saturation level after a strain of about 0.25, while in the two-phase alloy due to precipitate ripening all dislocation densities reveal a maximum, but do not attain a steady-state value within the tested strain regime. In general, dislocation densities are about three to five times higher for the two-phase alloy than for the sin-

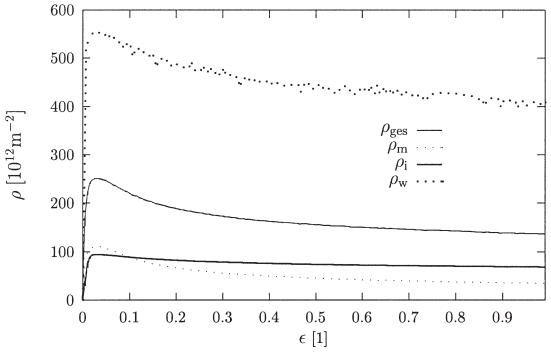

Fig. 7. Modelled dislocation densities for $\dot{\epsilon} = 1\times10^{-3}$ s^{-1} and $T = 350°$ C. Precipitation-hardened aluminium alloy (Al–4.16 wt% Cu–1.37 wt% Mg, AlCuMg2).

gle-phase alloy. Even though the dislocation density in the cell interiors is in both cases significantly lower than that in the cell walls, the cell interiors do significantly contribute to the total dislocations density and, therefore, to the flow stress as their volume fraction is 90%. In the single-phase alloy the mobile dislocation density amounts to only 7% of the total dislocation density, while in the two-phase alloy almost 30% of the total dislocation density are mobile dislocations.

3.5. Implementation in FE codes

The model presented readily lends itself to implementation in FE codes. Owing to the formation of flow stress development in terms of differential microstructural evolution equations, the spatial and temporal changes of the flow stress can be used to update the properties of any specific finite element. Of course, the strain used in the model corresponds to the von Mises equivalent strain as conventionally output from FE codes. A particular advantage of the hardening model is the explicit use of the number of activated slip systems for dynamic recovery to account for texture effects besides the macroscopic Taylor factor. This is particularly useful for advanced FE codes based on crystal plasticity.

In fact, interactive work hardening and FE computations of the rolling process have been conducted and reported elsewhere [24]. From the results it is obvious that the predictions of stress distribution in the rolling gap from this model are quite different from FE computations that utilize empirical power-law relations for the flow stress. First estimates of rolling forces and material temperature at roll exit confirm an improved prediction by the microstructural 3IVM.

The need for consideration of internal state variables to improve FE codes has also stimulated the development of micromechanical models like the Robinson and Bartolotta [1] or Chaboche [2] model, which consider the evolution of an internal state variable as well, e.g., in terms of an internal stress. Microstructural models like the approach presented here and micromechanical models may give numerically equivalent results for the prediction of flow stress. However, microstructural models will eventually be superior due to the explicit use of crystal plasticity mechanisms and, therefore, a physical reasoning and definition of bounds for the adjustable parameters. This becomes particularly significant upon change of material chemistry.

The evolution equation for the considered dislocation densities are defined in differential form and, therefore, are genuine for computation of non-stationary processes, e.g., change of strain path or temperature. In contrast, the temporal evolution of precipitation is presented only in an integral form in Section 2.2.3 [equations (22) and (23)] which precludes treatment of strong temperature changes. To account for such processing conditions incremental growth of precipitates has to be summed up for each element in all consecutive time steps. An explicit differential formulation is given elsewhere [25].

4. CONCLUSION

A new microstructural strain-hardening model of polycrystals is introduced based on three internal state variables. Three dislocation populations are distinguished: mobile dislocations and immobile dislocations both in cell walls and the cell interior. Precipitation and ripening of second-phase particles are considered—for isothermal conditions—via their influence on the mean free path of the mobile dislocations. By comparison of the behaviour of a two-phase commercial alloy with a precipitate-free model alloy, it was shown that the model is capable of adequately predicting the stress–strain curves of two-phase aluminium alloys at elevated temperatures. The model lends itself as a material constitutive law in FEM simulations. As the number of active slip systems is explicitly used in the evolution laws for the dislocation densities, the model is particularly suited for crystal plasticity FE simulations.

Acknowledgements—One of the authors (D. R.) gratefully acknowledges the financial support by the Deutsche Forschungsgemeinschaft through the Heisenberg program.

REFERENCES

1. Robinson, D. N. and Bartolotta, P. A., *NASA CR 174836*. National Aeronautics and Space Administration, Washington, DC, 1985.
2. Chaboche, J. L., *J. Appl. Mech.*, 1993, **60**, 813.
3. Kocks, U. F., *J. Eng. Mater. Technol.*, 1976, **98**, 72.
4. Mecking, H. and Kocks, U. F., *Acta metall.*, 1981, **29**, 1865.
5. Estrin, Y. and Mecking, H., *Acta metall.*, 1984, **32**, 57.
6. Gottstein, G. and Argon, A. S., *Acta metall.*, 1987, **35**, 1261.
7. Mughrabi, H., *Acta metall.*, 1983, **31**, 1367.
8. Mughrabi, H., *Mater. Sci. Eng.*, 1987, **85**, 15.
9. Prinz, F. B. and Argon, A. S., *Acta metall.*, 1984, **32**, 1021.
10. Zehetbauer, M. and Seumer, V., *Acta metall. mater.*, 1993, **41**, 577.
11. Zehetbauer, M., *Acta metall. mater.*, 1993, **41**, 589.
12. Argon, A. S. and Haasen, P., *Acta metall. mater.*, 1993, **41**, 3289.
13. Estrin, Y., Tóth, L. S., Molinari, A. and Bréchet, Y., *Acta mater.*, 1998, **46**, 5509.
14. Granato, A. V., Lücke, K., Schlipf, J. and Teutonico, L. J., *J. Appl. Phys.*, 1964, **35**, 2732.
15. Tome, C., Canova, G. R., Kocks, U. F., Christodoulou, N. and Jonas, J. J., *Acta metall.*, 1984, **32**, 1637.
16. Kratochvíl, J. and Libovický, S., *Scripta metall.*, 1986, **20**, 1625.
17. Reichert, B., Estrin, Y. and Schuster, H., *Scripta mater.*, 1998, **38**, 1463.
18. Lifshitz, I. M. and Slyozov, V. V., *J. Phys. Chem. Solids*. 1961, **19**, 35.
19. Wagner, C., *Z. Elektrochem.*, 1961, **65**, 581.
20. Wert, C. and Zener, C., *J. Appl. Phys.*, 1959, **21**, 5.
21. Essmann, U. and Mughrabi, H., *Phil. Mag. A*. 1979, **40**, 731.

22. Tippelt, B., Bretschneider, J. and Hähner, P., *Phys. Stat. Sol. (a)*. 1997, **163**, 11.
23. Kocks, U. F. and Canova, G. R., in *Deformation of Polycrystals*. ed. N. Hansen, A. Horsewell, T. Leffers and H. Lilholt. Risø National Laboratory, Roskilde, Denmark, 1981, p. 35.
24. Luce, A., Wolske, M., Kopp, R., Marx, V., Roters, F. and Gottstein, G., in *Proceedings of 4th International Conference on Recrystallization and Related Phenomena*. ed. T. Sakai and H. G. Suzuki, *JIM Proceedings*. Vol. 13. The Japan Institute of Metals, Sendai, Japan, 1999, p. 739.
25. Roters, F., Raabe, D., Löchte, L. and Gottstein, G., to be published.